ACS OMEGA

Open Access

http://pubs.acs.org/journal/acsodf

Article

Phosphate-Based Dechlorination of Electrorefiner Salt Waste using a Phosphoric Acid Precursor

Paige Murray, Harmony Werth, Sean Sullivan, Brian J. Riley, Michael Simpson, Charmayne Lonergan, and Krista Carlson*

Cite This: *ACS Omega* 2024, 9, 19395−19400

Read Online

ACCESS | Metrics & More | Article Recommendations

ABSTRACT: Electrochemical processing of spent nuclear fuel in molten chloride salts results in radioactive salt waste. Chlorine removal from the salt has been identified as an effective and efficient first step in the management of high-level waste. In this work, a simple salt was dechlorinated with a phosphoric acid phosphate precursor, resulting in a glassy dechlorinated product. The dechlorination efficacy was evaluated in air and argon environments. This work serves as an initial step to advance the Technological Readiness Level of H_3PO_4-based dechlorination step toward implementation of iron phosphate waste forms to immobilize electrochemical fuel reprocessing salt waste streams.

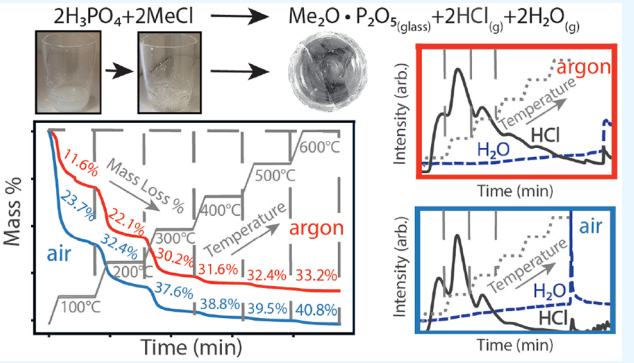

1. INTRODUCTION

Electrochemical processing has been ongoing since 1996 to treat irradiated driver fuel from Experimental Breeder Reactor-II (EBR-II) and Fast Flux Test Facility (FFTF) in the Fuel Conditioning Facility (FCF) at the Materials and Fuels Complex (MFC) of Idaho National Laboratory (INL, previously known as Argonne National Laboratory-West).[1,2] In the process graphically depicted in Figure 1a, U−Zr alloy-based fuel pins are chopped and electrorefined in a high temperature electrorefiner (ER) with an electrolyte composed of molten eutectic LiCl-KCl with 5 to 10 wt % UCl_3.[3] Uranium metal is recovered on the cathode and can be used to fabricate high assay low enriched uranium (HALEU) fuel for certain types of advanced reactors. With each batch of fuel electrorefined, certain active metal fission products further accumulate in the molten salt electrolyte. When fission product concentrations become too high for continued electrorefining operations, contaminated salt will need to be removed and replaced with eutectic LiCl-KCl and UCl_3. The total mass of waste salt projected to be generated from electrorefining of EBR-II and FFTF fuel in FCF is estimated to be in the range of 1.5−1.7 MT[5] and requires long-term storage and immobilization. The baseline process for immobilization of ER salt is the formation of glass-bonded sodalite.[6,7] The drawback of this process is that it multiplies the mass of salt waste by more than an order of magnitude. There has been much interest in developing higher salt-loaded waste forms.[8] One general approach is to dehalogenate the salt and immobilize the metals, since most of the radioactive elements are metals. Halogen species in the salt waste will likely include long-lived and low-activity waste components (e.g., ^{129}I with $t_{1/2}$ = 1.57 ×

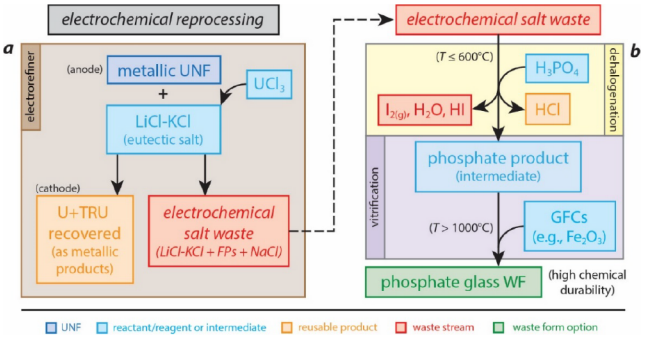

Figure 1. (a) Electrorefining process resulting in salt waste with fission products and the (b) two-step waste form process of dechlorination (or dehalogenation) and vitrification. This figure was modified from the original by Riley et al.[14] and was reprinted with permission from Riley, B. J.; Peterson, J. A.; Vienna, J. D.; Ebert, W. L.; Frank, S. M. *J. Nucl. Mater.* **2020**, 529, 151949. Copyright 2020 Brian J. Riley.

Received: January 17, 2024
Revised: March 4, 2024
Accepted: April 2, 2024
Published: April 16, 2024

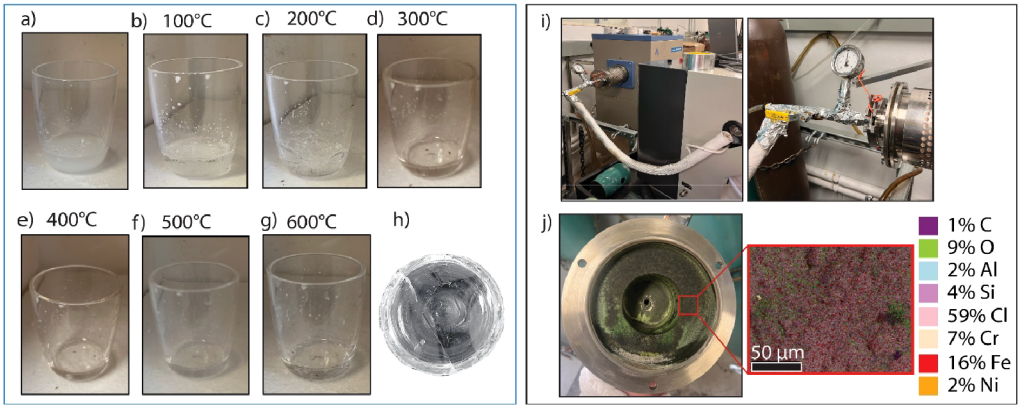

Figure 2. (a)−(g) Photographs taken during dechlorination reactions in air; (a) salt and phosphoric acid slurry immediately after mixing at room temperature, (b)−(g) during the ramp to the temperature labeled above the picture, (h) final dechlorinated product at $T > 300$ °C. (i) The atmosphere-controlled tube furnace connected to evolved gas analyzer. (j) Corrosion on the 304 stainless steel end-caps, with energy dispersive X-ray spectroscopy showing the approximate composition of the corrosion product.

10^7 y, ^{36}Cl with $t_{1/2}$ = 3.01 × 10^5 y) but can be treated separately for disposal or recycled back into the process. Several methods that evolve HCl as a byproduct of dechlorination have been explored. For example, Wasnik et al. reported successful dechlorination of eutectic LiCl-KCl via ion exchange with ultrastable H−Y zeolite.[9] Likewise, oxalic acid ($H_2C_2O_4$) was used successfully by Dong et al. as a dechlorination agent for the chlorine salt waste stream simulant ERV2.[10]

Another dehalogenation approach utilizes phosphate compounds[10] $(NH_4)_2HPO_4$ to remove halogens.[11−18] The main benefits of dehalogenation with phosphates are: the significant reduction in (or elimination of) the Cl from the salt that must be immobilized in the final waste form,[14−16] the ease of transformation of the phosphate into a glass-based waste form, and the recovery of the Cl as HCl or NH_4Cl that can subsequently be used in the transformation of metallic uranium into UCl_3 for advanced reactors.[19−22]

In the phosphate-based dehalogenation process, salt waste is reacted with a phosphate precursor at 300−600 °C to produce a glassy phosphate product containing salt cation oxides and to volatilize the chlorine species (e.g., HCl, NH_4Cl) as a byproduct that can be captured and potentially recycled (Figure 1b).[23] For a monovalent metal chloride (MeCl) reacted with H_3PO_4, the reaction proceeds as shown in eq 1.

$$2H_3PO_4 + 2MeCl \rightarrow Me_2O{\cdot}P_2O_{5(glass)} + 2HCl_{(g)} + 2H_2O_{(g)} \quad (1)$$

Similar reactions can occur with salts of monovalent and divalent cations. Because the intermediate phosphate glasses produced from this reaction are not chemically durable, glass modifiers and intermediates (e.g., Fe_2O_3, Al_2O_3) are added to increase the chemical durability of the final waste form following vitrification.[14,24−33]

As mentioned above, Cl removal from the salt waste stream aides in the waste form process as Cl solubility in oxide glasses tends to be very low and Cl concentrations are very limited for mineral waste forms such as sodalite[34−36] and apatite.[34,37] A benefit of Cl removal is that it can also be captured and recycled. The reason that Cl capture/recycle is of interest revolves around the application of molten salt reactors (MSRs) where ^{37}Cl-enriched salts could be used to prevent neutron activation of ^{35}Cl to ^{36}Cl, a long-lived radioisotope ($t_{1/2}$ = 3.01 × 10^5 y). Thus, if ^{37}Cl-enriched byproducts can be captured, they can be used to create the next phase of chloride-based MSR electrolyte salts. Otherwise, the halogen byproducts can be immobilized in a different waste form (e.g., sodalite) or discarded, depending on the level of radioactivity present.

However, the reaction of nitrogen-containing compounds (e.g., $NH_4H_2PO_4$) with halogen-containing streams can lead to the production of hazardous chemicals (e.g., HCl) and shock-sensitive contact explosives (e.g., NCl_3).[38] Thus, to avoid the latter, H_3PO_4 can be used, as it is a nitrogen-free phosphate dehalogenation agent. As this process is currently being considered for dechlorination of the electrorefining salt from EBR II,[39] this research is aimed to further investigate the use of H_3PO_4-based dechlorination to fill in the knowledge gaps and advance this technology toward a higher Technology Readiness Level. This need was defined in a recent roadmap report summarizing the technology gaps to advance the phosphate process for treating used electrochemical processing salt wastes.[40]

Two main areas were identified as in need for exploration: (1) tailoring the type and concentration of raw materials to maximize dechlorination of the starting salt while minimizing the formation of water and (2) determining the maximum extent of dechlorination in both air and argon atmospheres. Regarding the first area, the reactions between the aqueous phosphoric acid and the salt are complicated (e.g., time−temperature relationships for dehydration and HCl production and the role of H_2O in these reactions). For the second area, it is still unknown if this process will be implemented into a hot cell with an air or argon environment. Given that all the reported dechlorination experiments have been conducted in air, it was unknown how the absence of oxygen in the environment would alter the dechlorination efficacy. Based solely on the predictive reactions based on thermodynamics, it was postulated that additional oxygen from the atmosphere around the reaction would be required to fully convert the salt cations from halides to oxides. This study acted as an initial step to answering these questions.

https://doi.org/10.1021/acsomega.4c00542
ACS Omega 2024, 9, 19395−19400

2. EXPERIMENTAL SECTION AND ANALYSIS METHOD

Dechlorination studies were conducted using a simple salt mixture of 48LiCl-33KCl-19NaCl mol % (Thermo Scientific; ≥98.5%, 99%, and ≥99%, respectively). This salt ratio was selected to simulate spent ER salt composed of a LiCl-KCl eutectic composition with close to the maximum concentration of NaCl before salt replacement.[4] The individual salts were weighed inside a glovebox and placed in a silica crucible (AdValue Tech, FQ-1050). The salt mixture was then removed from the glovebox and placed in a fumehood, and H_3PO_4 (Fisher Chemical; 85%) was immediately added. The 10 g batch was mixed with a silica stirring rod for approximately 10 s, or until homogeneous, before being placed in the furnace for dechlorination (Figure 2a). Dechlorination was performed in an atmosphere-controlled tube furnace in either ultrazero air (2 ppm of H_2O, 0.5 ppm of CO_2) or ultrahigh purity argon (99.999%) with different temperature conditions. Samples were allowed to cool in the furnace to room temperature before being removed from the crucible for analysis.

3. RESULTS AND DISCUSSION

Initially, visual observations were recorded during dechlorination in a muffle furnace heated at a rate of 5 °C min^{-1}, with 1 h isothermal holds every 100 °C, up to a final temperature of 600 °C (Figure 2b–g). Large bubbles were consistently forming between 100 and 300 °C, indicating significant gas evolution in this temperature range (Figure 2b–d). Samples processed at 100 °C had the same slurry consistency as the original salt and phosphoric acid mixture (Figure 2a). Samples processed at T < 300 °C in argon stuck to the silica crucible and were tacky, thus preventing scanning electron microscopy (SEM)/energy dispersive X-ray spectroscopy (EDS) analysis. At T > 300 °C in argon or T > 200 °C in air, samples were removed easily from the crucible, typically as a single rigid monolith (Figure 2h). No fracture of the crucible was observed for samples processed between 100 and 400 °C. At 600 °C, about 67% of the silica crucibles would break during cooling in air atmosphere. No crucible breakage was observed in an argon atmosphere. The reason for the crucible breakage in air atmosphere is a topic of ongoing investigation, but is thought to be related to corrosion of the silica crucible during the phosphoric acid-based dechlorination process.

Thermogravimetric analysis (TGA; TA Instruments STD 650) was performed on small aliquots (~32 mg) of the simulated salt and phosphoric acid mixture in premium alumina pans (DSC Consumables, 90 mL, Q600). Two runs were performed for each environment and heating profile. The flow rate of the gas through the chamber during testing was 100 mL min^{-1}. The TGA curves for both air and argon atmospheres are shown in Figure 3. The TGA data shows that the majority of the mass loss (~98% in air and argon) occurred by 400 °C with less than 2% occurring between 400 and 600 °C. Dechlorination in air had ~12% greater mass loss than in argon in the first 100 °C. The mass loss became more similar as the temperature increased with a total difference in mass loss of 7.6% by 600 °C. Mass balance calculations for full dechlorination based on the dechlorination reaction shown in eq 1 agreed with this mass loss within 1% in air. Oxygen present in the air atmosphere is expected to aid in the conversion of salt cation chlorides to oxides and assist in the dechlorination process. It appears that the mass loss for each

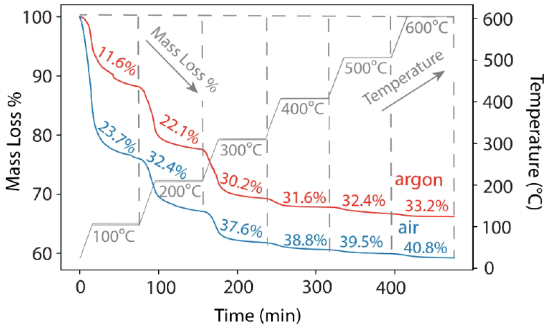

Figure 3. Percent mass loss in air and argon during heating to 600 °C with isothermal holds every 100 °C. Runs were performed in duplicate to confirm performance and within fractions of percent.

step had stabilized within the first 30 min, showing the potential for shorter isothermal holds or a continuous heating rate.

EDS (Thermo Fisher Scios 2 with EDAX Octane) analysis was performed on 10 g of dechlorinated products produced at 300–600 °C in either air or Ar with a flow rate of 150 mL min^{-1} (Figure 4). All products processed in air at T > 200 °C appeared transparent, and less than 0.6% Cl was observed. At 600 °C, no Cl was detected. The P, Na, and K were found in ratios close to what is expected for complete dechlorination. In Ar, products produced at T < 300 °C were tacky due to residual unreacted phosphoric acid reagent and could not be analyzed using EDS. Residual salt products were also suspended throughout the product. While products were "dry" after processing at 400 °C, residual salt particles were still observed (Figure 4b,c). The salt chunks appeared to be composed of NaCl, KCl, or a combination of the two. Since lithium chloride is deliquescent, it is postulated that Li was easily dissolved in the phosphoric acid and was more readily incorporated in the structure of the phosphate glass. At 600 °C, ~0.4 wt % Cl was detected; the amorphous XRD trace (Figure 5) indicates that this low level of chlorine remaining was accommodated by the alkali phosphate glass structure. As these samples were processed in static conditions, it is thought that agitation could assist with dissolution of the reagents and accelerate dechlorination.

Figure 5 shows the results from powder X-ray diffraction (XRD; Rigaku, SmartLab). Rigaku PDXL Software Version 2.0.3.0 was used to identify crystalline phases. All products formed in air were X-ray amorphous at T > 200 °C. Product formed at 600 °C in Ar was also X-ray amorphous. Product formed at 400 °C in Ar showed the presence of halite (NaCl, PDF 01–072–1668), which supports the EDS results. Product formed at 300 °C in Ar showed halite and additional phases matching sylvine (KCl, PDF 01–076–3364) and sylvine, sodian ($[Na_2K_8]Cl$, PDF 01–076–3393). No phases containing Li were detected in either sample.

An evolved gas analyzer (EGA; Extrel MAX300-EGA) was used to determine the concentrations of HCl and H_2O evolved during dechlorination. Samples were mixed and placed inside an atmosphere-controlled tube furnace attached to the EGA (Figures 2i,j). Prior to the start of the heating profile, samples were exposed to either flowing air or Ar for 3 h to allow the EGA signals to stabilize prior to analysis. Figure 6 shows the HCl and H_2O evolution results. For both air and Ar, the main release of HCl gas occurs during the ramping period from 200 to 300 °C with maximum losses occurring at ~70, ~ 119, and

https://doi.org/10.1021/acsomega.4c00542
ACS Omega 2024, 9, 19395–19400

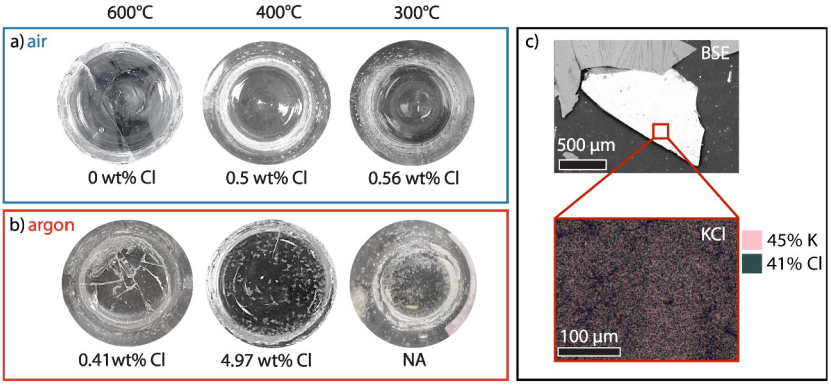

Figure 4. Photographs showing the dechlorinated phosphate products processed in (a) air and (b) argon. The bottom diameter of the crucible is 33 mm in optical photos. Residual chlorine for each dechlorinated product at temperature steps in air and argon is shown under the pictures. Products produced in air were transparent and homogeneous at all temperatures. Products produced in Ar had residual salt chunks that were heterogeneously distributed throughout the sample. No data could be collected on the product produced at 300 °C in Ar due to residual phosphoric acid. (c) EDS showing residual salt chunk composition and EDS analysis. Chunks were associated with Na, K, and Cl.

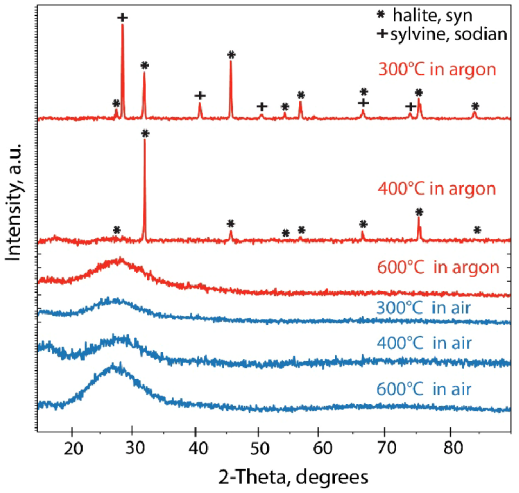

Figure 5. XRD patterns for dechlorinated products at temperatures between 300 and 600 °C in either air or argon. Scan parameters were 15−90° 2θ with a step of 0.07° 2θ and a scan step time of 1 s per step. All products were X-ray amorphous except for 400 °C in Ar in which halite (PDF 01−072−1668) was detected and 300 °C in Ar in which halite, sylvine (KCl PDF 01−076−3364) and sylvine, sodian (PDF 01−076−3393) were identified.

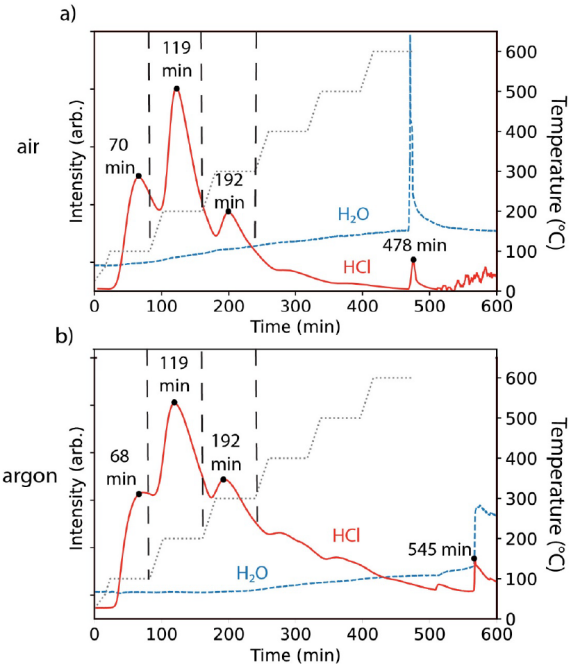

Figure 6. Evolved gas analyzer depicting gas release at a temperature in air (a) and argon (b). Heating profile was completed after 475 min, after which the furnace was shut off and allowed to naturally cool as gas flowed through the system. The HCl and H_2O returned to their background levels after ∼20 h.

∼192 min. The gas evolution time and temperature correspond well with the TGA data, despite the measurement time delay in the larger system. After 300 °C, the amount of HCl released gradually declined.

Although the time and temperature of HCl evolution are in good agreement with the TGA data, the absolute values for the off-gas species are not reported due to challenges associated with corrosion. The EGA detected a gradual increase in H_2O intensity during heating. However, a large spike in the H_2O intensity was observed after the heating profile had ended (475 min), and the furnace was programmed to cool: at 478 min for the sample in air and 545 min for the sample in Ar. Intensity spikes of this nature are indicative of a sudden release of previously trapped species into the EGA sampling port (0.13 mm diameter inlet). Some HCl was also trapped in this vapor but at significantly lower levels and is not thought to greatly impact the shape or intensity of the curves at $T < 300$ °C. Heat trace was used to minimize cooling (Figure 2i) to mitigate condensation of the gaseous species before sampling with the EGA. Unfortunately, the furnace tube end-cap (Figure 2j) was still significantly corroded by the acidic water vapor. EDS (Figure 2j) and XRD (not shown) analyses of the corrosion product revealed it to be iron chloride hydrate ($FeCl_2$-$4H_2O$, PDF 00−016−0123).

To mitigate corrosion, future experiments examining the dechlorination reactions were conducted in an apparatus made entirely of silica. Despite the corrosion-related issues, these findings are an important first step in understanding the off-gas and its impact on materials similar to those that will be used during full-scale processing. Although the exact evolution of water still needs to be determined, it was demonstrated that HCl is released primarily at early stages, indicating that the use

https://doi.org/10.1021/acsomega.4c00542
ACS Omega 2024, 9, 19395−19400

of isotherms may not be required to achieve full dechlorination.

4. CONCLUSIONS

In conclusion, the phosphate dechlorination process was successfully performed in both air and argon by using a phosphoric acid precursor. Atmospheric oxygen plays an important role in the dechlorination process as complete dechlorination is achieved at a lower temperature in air than in argon. To further advance the TRL, a deeper understanding of the salt/precursor compositions and processing conditions needs to be developed. Next steps include (1) quantifying of the concentration of gas species released during dechlorination in air and argon in static and dynamic conditions (e.g., in a rotating tube furnace), (2) determining the maximum salt loading for complete dechlorination, (3) determining how dechlorination efficacy changes with surrogate salts, and (4) evaluating the corrosivity of the off-gas on materials that will most likely be used in a processing facility. It will be critical to compare these results to dechlorination using other phosphate precursors (e.g., ADP) to assess the benefits and disadvantages of this method before scaling the process.

AUTHOR INFORMATION

Corresponding Author

Krista Carlson − *Department of Chemical and Materials Engineering, University of Nevada, Reno, Nevada 89557, United States;* orcid.org/0000-0002-4288-2641; Phone: 607-382-1769; Email: kc@unr.edu

Authors

Paige Murray − *Department of Chemical and Materials Engineering, University of Nevada, Reno, Nevada 89557, United States*

Harmony Werth − *Department of Chemical and Materials Engineering, University of Nevada, Reno, Nevada 89557, United States*

Sean Sullivan − *Department of Chemical and Materials Engineering, University of Nevada, Reno, Nevada 89557, United States*

Brian J. Riley − *Pacific Northwest National Laboratory, Richland, Washington 99352, United States;* orcid.org/0000-0002-7745-6730

Michael Simpson − *Department of Materials Science and Engineering, University of Utah Ringgold Standard Institution, Salt Lake City, Utah 84112-9057, United States*

Charmayne Lonergan − *Missouri University of Science and Technology Ringgold Standard Institution, Rolla, Missouri 65409, United States*

Complete contact information is available at: https://pubs.acs.org/10.1021/acsomega.4c00542

Author Contributions

P.M. was responsible for conceptualization, formal analysis, investigation, methodology, and writing—original draft; H.W. was responsible for the investigation and writing—original draft; S.S. was responsible for the investigation, writing—review and editing; B.J.R. was responsible for conceptualization, formal analysis, and writing—review and editing; M.S. was responsible for writing—review and editing; C.L. was responsible for writing—review and editing; K.C. was responsible for conceptualization, project administration, supervision, and writing—review and editing. The manuscript was written through contributions of all authors. All authors have given approval to the final version of the manuscript.

Notes

The authors declare no competing financial interest.

ACKNOWLEDGMENTS

This work was supported by the United States Department of Energy (DOE) Nuclear Energy University Program (NEUP) under contract DE-NE0009317, and the US Nuclear Regulatory Commission (USNRC) under contract 31310022M015. Pacific Northwest National Laboratory (PNNL) is operated by Battelle Memorial Institute for the DOE under contract DE-AC05−76RL01830. The authors thank Jarrod Crum for his review of the manuscript.

REFERENCES

(1) Lineberry, M. J.; Phipps, R. D.; Benedict, R. W.; Laidler, J. J.; Battles, J. E.; Miller, W. E. Fuel Cycle and Waste Management Demonstration in the IFR Program In *Proceedings of American Nuclear Society and the American Society of Mechanical Engineers*. CONF-920818−920816,1992.

(2) Till, C. E.; Chang, Y. I. *Plentiful Energy. The Story of the Integral Fast Reactor: the complex history of a simple reactor technology, with emphasis on its scientific bases for non-specialists*; Charles E. Till and Yoon Il Chang, 2011.

(3) Li, S. X.; Johnson, T. A.; Westphal, B. R.; Goff, K. M.; Benedict, R. W. *Electrorefining experience for pyrochemical reprocessing of spent EBR-II driver fuel, INL/CON-05−00305*; Idaho National Laboratory: Idaho Falls, ID, 2005.

(4) Carlson, K.; Gardner, L.; Moon, J.; Riley, B. J.; Amoroso, J. M.; Chidambaram, D. Molten salt reactors and electrochemical reprocessing: synthesis and chemical durability of potential waste forms for metal and salt waste streams. *Int. Mater. Rev.* **2021**, *66* (5), 339−363.

(5) Simpson, M. F.; Barber, D. B.; Benedict, R. W.; Teske, G. M. *EBR-II and FFTF Spent Fuel Processing Options Report*; Idaho National Laboratory: Idaho Falls, ID, 2006.

(6) Priebe, S.; Bateman, K. The ceramic waste form process at the Idaho National Laboratory. *Nucl. Technol.* **2008**, *162* (2), 199.

(7) Simpson, M. F.; Goff, K. M.; Johnson, S. G.; Bateman, K. J.; Battisti, T. J.; Toews, K. L.; Frank, S. M.; Moschetti, T. L.; O'Holleran, T. P.; Sinkler, W. A Description of the Ceramic Waste Form Production Process from the Demonstration Phase of the Electrometallurgical Treatment of EBR-II Spent Fuel. *Nucl. Technol.* **2001**, *134*, 263.

(8) Riley, B. J. Electrochemical salt wasteform development: A review of salt treatment and immobilization options. *Ind. Eng. Chem. Res.* **2020**, *59*, 9760.

(9) Wasnik, M. S.; Grant, A. K.; Carlson, K.; Simpson, M. F. Dechlorination of molten chloride waste salt from electrorefining via ion-exchange using pelletized ultra-stable H-Y zeolite in a fluidized particle reactor. *J. Radioanal. Nucl. Chem.* **2019**, *320*, 309.

(10) Dong, Y.; Xu, K.; Jia, Z.; Niu, C.; Xu, D. Dechlorination and vitrification of electrochemical processing salt waste. *J. Nucl. Mater.* **2022**, *567*, 153833.

(11) Donze, S.; Montagne, L.; Palavit, G. Thermal conversion of heavy metal chlorides ($PbCl_2$, $CdCl_2$) and alkaline chlorides (NaCl, KCl) into phosphate glasses. *Chem. Mater.* **2000**, *12*, 1921.

(12) Siemer, D. D. Improving the integral fast reactor's proposed salt waste management system. *Nucl. Technol.* **2012**, *178*, 341.

(13) Frank, S. M.; Riley, B. J.; Ebert, W. L.; Peterson, J. A. *Literature Review of Dehalogenation Processes for Salt Wastes and Suitable Waste Forms, NTRD-MRWFD-2017−000193*; Idaho National Laboratory: Idaho Falls, ID, 2017.

(14) Riley, B. J.; Peterson, J. A.; Vienna, J. D.; Ebert, W. L.; Frank, S. M. Dehalogenation of electrochemical processing salt simulants with

https://doi.org/10.1021/acsomega.4c00542
ACS Omega 2024, 9, 19395−19400

ammonium phosphates and immobilization of salt cations in an iron phosphate glass waste form. *J. Nucl. Mater.* **2020**, *529*, 151949.
(15) Riley, B. J.; Chong, S.; Lonergan, C. E. Dechlorination Apparatus for Treating Chloride Salt Wastes: System Evaluation and Scale-Up. *ACS Omega* **2021**, *6*, 32239.
(16) Lee, K. R.; Riley, B. J.; Park, H.-S.; Choi, J.-H.; Han, S. Y.; Hur, J.-M.; Peterson, J. A.; Zhu, Z.; Schreiber, D. K.; Kruska, K.; et al.etal. Investigation of physical and chemical properties for upgraded SAP (SiO_2-Al_2O_3-P_2O_5) waste form to immobilize radioactive waste salt. *J. Nucl. Mater.* **2019**, *515*, 382.
(17) Park, H.-S.; Kim, I.-T.; Cho, Y.-Z.; Eun, H.-C.; Lee, H.-S. Stabilization/solidification of radioactive salt waste by using $x$$SiO_2$-$y$$Al_2O_3$-$z$$P_2O_5$ (SAP) material at molten salt state. *Environ. Sci. Technol.* **2008**, *42*, 9357.
(18) Choi, E.-Y.; Jeong, S. M. Electrochemical processing of spent nuclear fuels: An overview of oxide reduction in pyroprocessing technology. *Progr. Nat. Sci.: Mater. Int.* **2015**, *25* (6), 572−582.
(19) Perhach, C.; Chamberlain, J.; Rood, N.; Hamilton, E.; Simpson, M. F. Chlorination of uranium metal in molten NaCl-$CaCl_2$ via bubbling HCl. *J. Radioanal. Nucl. Chem.* **2022**, *331*, 2303.
(20) Eun, H. C.; Kim, T. J.; Jang, J. H.; Kim, G. Y.; Lee, S. J.; Hur, J. M. A study on chlorination of uranium metal using ammonium chloride. *J. Radioanal. Nucl. Chem* **2017**, *314*, 533.
(21) Yoon, D.; Paek, S.; Lee, C. Chlorination of uranium metal to uranium trichloride using ammonium chloride. *J. Radioanal. Nucl. Chem.* **2022**, *331*, 2209.
(22) Herrmann, S. D.; Zhao, H.; Bawane, K. K.; He, L.; Tolman, K. R.; Pu, X. Synthesis and characterization of uranium trichloride in alkali-metal chloride media. *J. Nucl. Mater.* **2022**, *565*, 153728.
(23) Riley, B.; Peterson, J.; Vienna, J.; Ebert, W.; Frank, S. Dehalogenation of electrochemical processing salt simulants with ammonium phosphates and immobilization of salt cations in an iron phosphate glass waste form. *Nat. Prod. J. Nucl. Mater.* **2020**, *529*, 151949.
(24) Ebert, W. L.; Riley, B. J.; Peterson, J. A.; Frank, S. M. *Durability Testing of Developmental Iron Phosphate Waste Forms for Echem Salt Waste, NTRD-MRWFD-2018−000513*; Argonne National Laboratory: Lemont, IL, 2018.
(25) Ebert, W. L.; Fortner, J. A. *Corrosion Tests with Developmental Iron Phosphate Glass Waste Forms, ANL/CFCT-19/7*; Argonne National Laboratory: Lemont, IL, 2019.
(26) Ebert, W. L.; Fortner, J. A. *Corrosion Behavior of Developmental Iron Phosphate Glass Waste Forms, ANL/CFCT-20/1*; Argonne National Laboratory: Lemont, IL, 2020.
(27) Stariha, S. A.; Ebert, W. L. *Corrosion Behavior of Developmental Iron Phosphate Glass Waste Forms: fY20 Status Report, ANL/CFCT-20/34*; Argonne National Laboratory: Lemont, IL, 2020.
(28) Stariha, S. A.; Ebert, W. L. *Corrosion Behavior of Developmental Iron Phosphate Waste Forms: fY21 Status Report, ANL/CFCT-21/14*; Argonne National Laboratory: Lemont, IL, 2021.
(29) Ebert, W. *Conceptual Iron Phosphate Waste Form Degradation Model, ANL/CFCT-22/48*; Argonne National Laboratory: Lemont, IL, 2022.
(30) Stariha, S. A.; Ebert, W. L. *Corrosion Behavior of Fast-Cooled Iron Phosphate Reference Material, ANL/CFCT-22/49*; Argonne National Laboratory: Lemont, IL, 2022.
(31) Stariha, S. A.; Ebert, W. L. *Durability Assessments of Quenched and Slow-Cooled Iron Phosphate Waste Form Materials, ANL/CFCT-23/24*; Argonne National Laboratory: Lemont, IL, 2023.
(32) Riley, B. J.; Chong, S.; Peterson, M.; Nienhuis, E. T. *Aluminophosphate Waste Forms for Immobilizing Cations from Electrochemical Salt Wastes, PNNL-33906*; Pacific Northwest National Laboratory: Richland, WA, 2023.
(33) Riley, B. J.; Chong, S.; Nienhuis, E. T. *Canister Centerline Cooling Experiments for DPF5−336 Reference Material Made with ERV3b Salt Simulant, PNNL-33802*; Pacific Northwest National Laboratory: Richland, WA, 2023.
(34) Vance, E. R.; Davis, J.; Olufson, K.; Chironi, I.; Karatchevtseva, I.; Farnan, I. Candidate waste forms for immobilisation of waste chloride salt from pyroprocessing of spent nuclear fuel. *J. Nucl. Mater.* **2012**, *420*, 396.
(35) Riley, B. J.; Vienna, J. D.; Frank, S. M.; Kroll, J. O.; Peterson, J. A.; Canfield, N. L.; Zhu, Z.; Zhang, J.; Kruska, K.; Schreiber, D. K. Glass binder development for a glass-bonded sodalite ceramic waste form. *J. Nucl. Mater.* **2017**, *489*, 42.
(36) Riley, B. J.; Peterson, J. A.; Chong, S.; Vienna, J. D. Influence of ion site occupancies on the unit cell parameters, specific volumes, and densities of M8(AlSiO4)6X2 sodalites where M = Li, Na, K, Rb, and Ag and X = Cl, Br, and I. *Phys. Chem. Miner.* **2021**, *48* (1), 1−10.
(37) Metcalfe, B. L.; Donald, I. W.; Fong, S. K.; Gerrard, L. A.; Strachan, D. M.; Scheele, R. D. Calcium Phosphate: A Potential Host for Halide Contaminated Plutonium Wastes. *MRS Online Proc. Libr.* **2008**, *1124*, 1124−Q04−02.
(38) Riley, B. J.; Chong, S. Dehalogenation reactions between halide salts and phosphate compounds. *Front. Chem.* **2022**, *10*, 976781.
(39) Tolman, D. D.; Riley, B. J. *Conceptual Design of a Salt Dechlorination and Vitrification Apparatus (DeVA), INL/RPT-23−72319, PNNL-34755*; Idaho National Laboratory: Idaho Falls, ID, 2023.
(40) Riley, B. J.; Vienna, J. D.; Ebert, W. L. *Road Map for Developing Iron Phosphate Waste Forms for Salt Wastes, PNNL-30998, ANL/CFCT-20/44*; Pacific Northwest National Laboratory: Richland, WA, 2021.

https://doi.org/10.1021/acsomega.4c00542
ACS Omega 2024, 9, 19395−19400